

POLARIZED LIGHT IMAGING OF THE HD 142527 TRANSITION DISK WITH THE GEMINI PLANET IMAGER: DUST AROUND THE CLOSE-IN COMPANION*

TIMOTHY J. RODIGAS^{1,4}, KATHERINE B. FOLLETTE², ALYCIA WEINBERGER¹, LAIRD CLOSE², DEAN C. HINES³

Draft version May 24, 2021

ABSTRACT

When giant planets form, they grow by accreting gas and dust. HD 142527 is a young star that offers a scaled-up view of this process. It has a broad, asymmetric ring of gas and dust beyond ~ 100 AU and a wide inner gap. Within the gap, a low-mass stellar companion orbits the primary star at just ~ 12 AU, and both the primary and secondary are accreting gas. In an attempt to directly detect the dusty counterpart to this accreted gas, we have observed HD 142527 with the Gemini Planet Imager in polarized light at Y band ($0.95\text{--}1.14\ \mu\text{m}$). We clearly detect the companion in total intensity and show that its position and photometry are generally consistent with the expected values. We also detect a point-source in polarized light that may be spatially separated by \sim a few AU from the location of the companion in total intensity. This suggests that dust is likely falling onto or orbiting the companion. Given the possible contribution of scattered light from this dust to previously reported photometry of the companion, the current mass limits should be viewed as upper limits only. If the dust near the companion is eventually confirmed to be spatially separated, this system would resemble a scaled-up version of the young planetary system inside the gap of the transition disk around LkCa 15.

Subject headings: instrumentation: adaptive optics — techniques: high angular resolution — stars: individual (HD 142527) — circumstellar matter — planetary systems

1. INTRODUCTION

HD 142527 (spectral type F6 IIIe, Houk 1978; age = 5 ± 1.5 Myr, distance = 140 ± 20 pc, Mendigutía et al. 2014) is a young Herbig Ae/Be star with a complex circumstellar environment. It hosts a wide circumstellar disk, consisting of both dust and gas, located beyond ~ 100 AU (Fukagawa et al. 2006). Within 100 AU, the dust and gas density decline rapidly, revealing an apparent gap. An inner disk is also thought to exist beyond $\sim 5\text{--}10$ AU, but its outer extent is not well-constrained (Verhoeff et al. 2011; Nagel 2014). The surface of the outer disk may contain water ice (Honda et al. 2009)—thought to be an essential ingredient for giant planet formation (Kokubo & Ida 2002). Recently Biller et al. (2012) interferometrically detected a low-mass stellar companion within the inner disk, and Close et al. (2014) directly imaged the $\sim 0.25\ M_{\odot}$ companion using Magellan adaptive optics (MagAO) by detecting a strong H α emission line that indicates gas accretion. Interestingly, Casassus et al. (2013b) detected gaseous streamers that appear to be crossing the disk gap on the opposite side of the companion, suggesting that both the primary and secondary stars are accreting gas from inside the gap, where warm gas is thought to exist (Casassus et al. 2013a).

These recent findings raise several important questions: Is the secondary responsible for creating the wide gap?

Since it is accreting gas, does it also have a *circumsecondary* disk of dust? If it is surrounded by dust, did the dust originate in the inner or outer disk? To address these questions, high-contrast imaging capable of detecting dust at $< 0''.1$ is required. In this Letter, we report the direct detection of HD 142527B at Y band ($0.95\text{--}1.14\ \mu\text{m}$) in total intensity, along with an offset source of polarized light, suggesting that dust is falling onto or orbiting the companion.

2. OBSERVATIONS AND DATA REDUCTION

Observations of HD 142527 were carried out using the Gemini Planet Imager (GPI; Macintosh et al. 2012) on the Gemini-South Telescope at Cerro Pachon, Chile on the night of UT 25 April 2014 as part of the Early Science campaign. Images were obtained in polarized light at Y band. GPI has a plate scale of 14.14 ± 0.01 mas/pixel (Konopacky et al. 2014) and a field of view of $2''.8$ on a side. Observing conditions were good, with seeing at or below $0''.75$ for most of the night. To minimize the radial extent of saturation on the detector, we used the shortest possible integration time of 1.5 s and coadded 10 of these frames (15 s total per image). One image was obtained at each of the following half-wave plate angles: 0° , 45° , 22° , 67° ⁶, and then the sequence was repeated until 50 images were obtained, resulting in a total integration of 12.12 minutes. The instrument pupil was fixed during the observations, resulting in a total field of view rotation on the detector of 29.75° and enabling angular differential imaging (ADI; Marois et al. 2006). A PSF reference star, HIP 82885, was imaged immediately afterwards using the same instrumental setup for a total integration of 2.9 minutes. Images of HD 142527 were saturated within

* This paper includes data obtained at the Gemini-South telescope using the Gemini Planet Imager.

¹Department of Terrestrial Magnetism, Carnegie Institute of Washington, 5241 Broad Branch Road, NW, Washington, DC 20015, USA; email: trodigas@carnegiescience.edu

³Space Telescope Science Institute, Baltimore, MD 21218, USA

²Steward Observatory, The University of Arizona, 933 N. Cherry Ave., Tucson, AZ 85721, USA

⁴Carnegie Postdoctoral Fellow

⁶At the time of the observations, the Gemini Phase II software was incompatible with half-angle increments such that 22.5° and 67.5° were set to integer values.

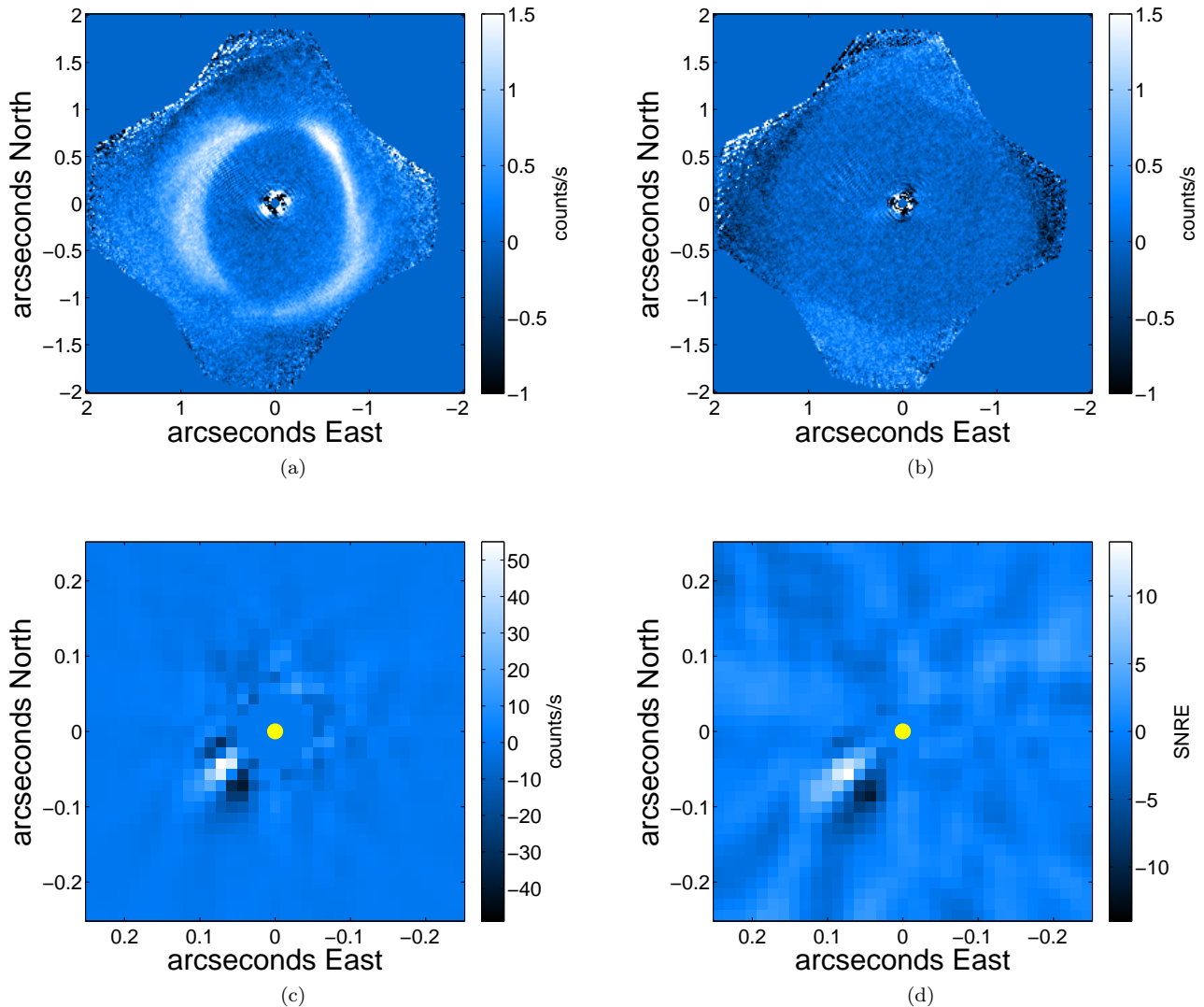


FIG. 1.— (a): PDI-processed P_{\perp} image of the outer disk at Y band. The outer disk is easily recovered. (b): PDI-processed P_{\parallel} image, which contains \sim zero signal at the location of the outer disk, as expected. (c): Zoomed-in total intensity image, obtained by reducing the data using ADI+PCA. The known companion, HD 142527B, is detected near its expected location. The negative residuals on either side of the companion are caused by self-subtraction in the ADI+PCA reduction. The yellow dot in this and other figures represents the location of the primary star. (d): SNRE map showing that the companion is detected at $S/N \sim 14$.

0 $^{\circ}$:05; images of the PSF reference star were not saturated (though some pixels were in the non-linear regime⁷).

We used the GPI IDL data reduction package (v. 1.1)⁸ to split each raw image into a datacube consisting of the ordinary and extraordinary beams. The processing pipeline locates the two polarization spots created by each lenslet and then constructs one image for each orthogonal polarization state. It also corrects for bad pixels and destripes the images.

Next we processed the images using our custom high-contrast imaging reduction routines written in Matlab. We divided each image by the number of coadds and the integration time to obtain units of counts/s. We then registered each image by calculating the center of light while ignoring saturated pixels. At this point, the

dataset consisted of 50 ordinary beam images and 50 extraordinary beam images.

To confirm the known outer disk structure, we followed the “double ratio” polarized differential imaging (PDI) method (see Avenhaus et al. 2014 and references therein for more details), which yields P_{\perp} , the tangential polarization flux, and P_{\parallel} , the radial polarization flux. For this near face-on disk, P_{\parallel} should contain \sim zero signal and is thus a measure of the noise. After constructing these image sets, we rotated the images by their parallactic angles plus an instrumental offset to obtain North-up, East-left. To compute this offset, we reduced GPI spectral calibration data taken earlier in the April observing run on the Theta 1 Ori multiple star system at H band. Using the known PA of the B₂-B₃ component from Close et al. (2013), which has very little proper motion over timescales of ~ 1 year, we determined that an additional 3 $^{\circ}$ of clockwise rotation was needed to

⁷ <http://www.gemini.edu/sciops/instruments/gpi/instrument-performance/detector-characteristics>

⁸ <http://docs.planetimager.org/pipeline/>

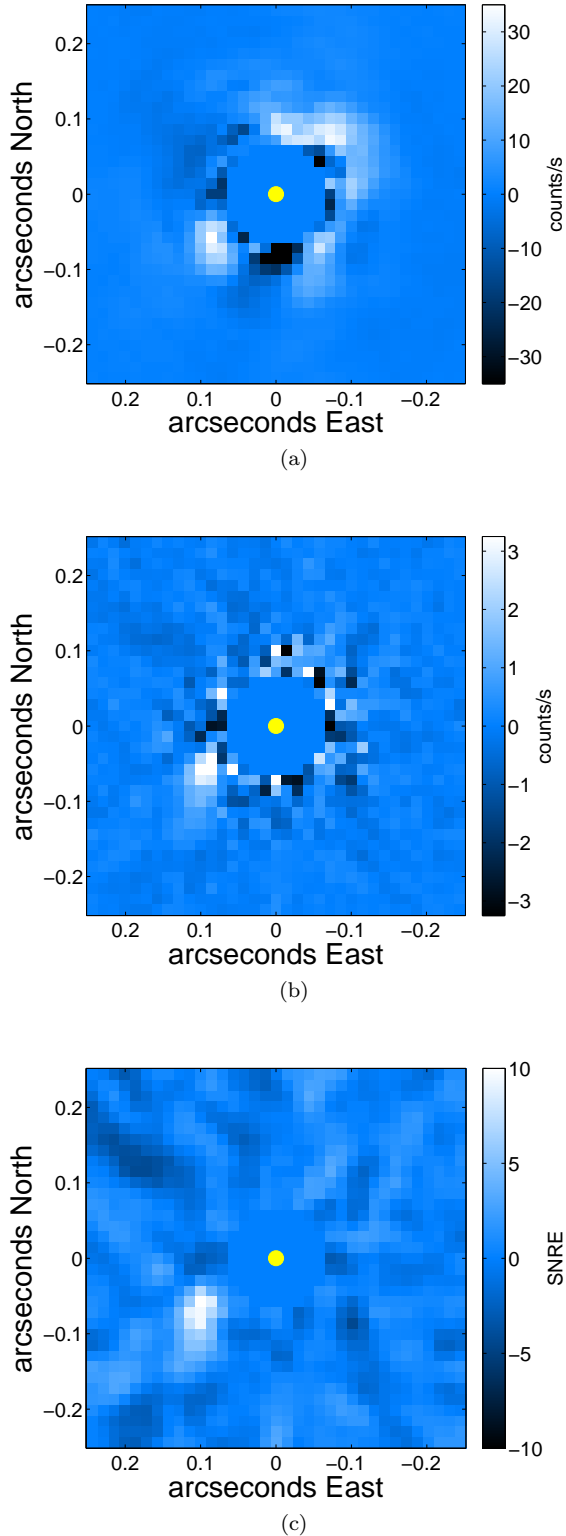


FIG. 2.— (a): Final zoomed-in P_{\perp} image generated using ODD, showing a bright point-source near the location of HD 142527B. (b): P_{\perp} image, after additional PSF subtraction using ADI+PCA. The source is clearly detected and all other artifacts are removed. (c): SNRE map, showing that the polarized source is detected at $S/N \sim 11$.

align the images with true North⁹. Fig. 1a and Fig. 1b show the final P_{\perp} and P_{\parallel} images, respectively. The outer disk is clearly detected at high S/N, and no similar structures are evident in the radial polarization image. Furthermore, the known polarization “holes” at position angles (PA) of $\sim 0^{\circ}$ and 160° (Avenhaus et al. 2014; Canovas et al. 2013) are recovered at approximately the same locations.

2.1. Recovering the companion in total intensity

To detect HD 142527B in total intensity, we first added the 50 ordinary beam images with the 50 extraordinary beam images, yielding 50 total intensity images. We then reduced this dataset using our custom ADI pipeline in combination with Principal Component Analysis (PCA; Soummer et al. 2012). We varied the number of modes used to generate the PSFs, rotated the images by their parallactic angles to obtain North-up, East-left, and combined them using a mean with sigma clipping. The final number of modes was 8 (out of 50), since this resulted in a point-source being detected at a maximum S/N per resolution element (SNRE)¹⁰ ~ 14 near the expected location of HD 142527B, based on the astrometry from Biller et al. (2012) and Close et al. (2014). The final total intensity image and the corresponding SNRE map are shown in Fig. 1c and Fig. 1d, respectively. These images, in particular the SNRE map, show that the object is radially extended, suggesting that additional signal resides *outside* the point-source.

2.2. Recovering polarized light near the companion

To determine whether any polarized light is being scattered from the circumsecondary environment of HD 142527B, we combined the “double difference” method (e.g., Kuhn et al. 2001; Hinkley et al. 2009) with the “double ratio” method. Specifically, we used PCA optimization to improve the PSF subtraction step in the former method and then used the latter method to correct for imperfect alignment of the half-wave plate (Avenhaus et al. 2014). We refer to the combined method employed here as Optimized Double Differencing (ODD), which we describe below.

Typically, double differencing starts by generating Q and U images, which themselves are the differences of the ordinary and extraordinary beam images taken at various half-wave plate angles. The ordinary and extraordinary beam images are taken simultaneously, so the unpolarized star light is a good representation of the PSF. To improve the PSF subtraction in this step, we generated an optimal PSF from all of the available extraordinary images at a given half-wave plate angle using PCA. In other words, for the 0° half-wave plate angle, a given Q image was generated using Eq. 1,

$$Q_i = O_i^{0^{\circ}} - PSF(E_{1:K}^{0^{\circ}}), \quad (1)$$

⁹ Konopacky et al. (2014) found a rotational offset closer to $\sim 1^{\circ}$; however, this was not computed using the Theta 1 Ori system.

¹⁰ This was computed by convolving the final image with a Gaussian of $\text{FWHM} = 38.2$ mas, masking out the companion and computing the standard deviations in 1 pixel wide annuli as a function of radius, then dividing the Gaussian-smoothed image by these noise values.

where $i \in [1, 12]$, with 12 being the number of images in a given half-wave plate sequence, O (E) refers to the ordinary (extraordinary) beam of the polarized image, PSF is the optimal PSF generated by PCA from the appropriate extraordinary images, and K is the number of modes used to construct the PSF (here = 12). $-Q$, U , and $-U$ were generated in a similar manner using the 45° , 22° , and 67° half-wave plate angle images, respectively.¹¹

The final Q and U images were computed in the normal manner (e.g., $Q - (-Q) = 2Q$). We then used the Q and U images to calculate P_\perp and P_\parallel , following the double ratio method (Avenhaus et al. 2014). At this point, if we rotate and combine the P_\perp images, we detect a bright point-source near the location of HD 142527B in total intensity (Fig. 2a). However, we can improve this detection by taking advantage of the ADI setup of the instrument and employing additional PSF subtraction on the (unrotated) P_\perp images. We again used PCA, this time with 3 modes (out of 12).¹² After PSF subtracting, we rotated the images by their parallactic angles to obtain North-up, East-left and combined the images using a mean with sigma clipping. The final image is shown in Fig. 2b, wherein the same point-source originally seen in Fig. 2a is now recovered at S/N ~ 11 (Fig. 2c), and all other artifacts have been removed. To check that the recovered source was not an instrumental polarization artifact, we repeated the above reduction on the P_\parallel images. The final image did not show any similar structures near the polarized source, validating the detection.

3. RESULTS

3.1. Astrometry

To compute the astrometry of the point-source in total intensity (Fig. 1c) and polarized intensity (Fig. 2b), we calculated the center of light in 3x3 pixel boxes centered on the brightest pixel near the location of the sources in each image. We assumed astrometric uncertainties of 0.5 pixels in the x and y directions, since GPI is just barely Nyquist-sampled at Y band¹³. In total intensity, the source has a separation from the primary of 88.25 ± 10.1 mas and PA of $123 \pm 9.2^\circ$. In polarized intensity, the source has a separation of 107.2 ± 10.1 mas and a PA of $121.84 \pm 7.56^\circ$. These locations are shown in Fig. 3, along with the previously published astrometry from 2012-2013 (Biller et al. 2012; Close et al. 2014). For reference we also plot the preliminary location of HD 142527B from MagAO/ $H\alpha$ observations repeated in April 2014 (separation = 79.7 ± 5.6 mas, PA = $119.5 \pm 8.17^\circ$; Follette et al., in prep.). The location of the source in total intensity from GPI generally agrees

¹¹ Because off-axis sources rotate throughout observations, the polarization signal also rotates. This means that double differencing will result in a potentially biased polarized signal, depending on the speed and magnitude of the sky rotation between images. In our case, this bias is expected to be small and is outweighed by the gain in final S/N using ODD.

¹² We note that the PSFs used in this step were generated from the images themselves. Since they contain the (rotating) companion in polarized light, the flux of any recovered signal will have been attenuated.

¹³ λ/D at Y band is 26.7 mas (1.9 pixels). By comparing the measured widths of inserted and recovered Gaussians with the width of the recovered companion, we found that the GPI PSF had a width of ~ 38.2 mas (2.67 pixels). This satisfies the Nyquist requirement.

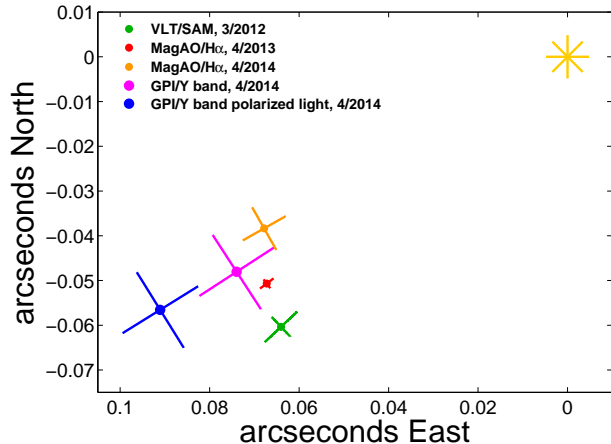


Fig. 3.— Astrometry of the HD 142527 circumstellar environment. The blue and pink points are the polarized and total intensity locations, respectively, from this work. The green point is the location from Biller et al. (2012) using Sparse Aperture Masking (SAM) with the VLT. The red point is the location from Close et al. (2014) using MagAO imaging at $H\alpha$, and the orange point is the preliminary location from the same observations repeated in April 2014 (Follette et al., in prep.). The yellow asterisk marks the location of the primary star.

with the expected location of HD 142527B based on orbital motion over the course of ~ 1 year. It is marginally discrepant with the new MagAO location, though at 1.4σ confidence. Thus we consider our source to be the companion. Interestingly, the projected separation of the polarized source is larger than that of the companion by ~ 19.2 mas = 2.7 AU, at $\sim 2\sigma$ confidence. However, this significance comes from the absolute astrometric uncertainty. Because both positions were measured in the same way using the same instrument, the *relative* uncertainty is likely much smaller, meaning 2σ is a lower limit.

3.2. Companion photometry in total intensity

We computed the companion photometry in total intensity by repeatedly inserting and recovering a scaled, mean-combined image of the unsaturated PSF, HIP 82885, at the same radius but $\sim 180^\circ$ away from the measured location of the companion. We varied the scale factor until the brightness of the artificial companion matched the measured brightness and S/N of the real companion (Fig. 4). Because the PSF image was non-linear in the central few pixels, we assumed a conservative uncertainty of 0.5 mag for the companion photometry. The optimal scale factor for the PSF was 0.055, corresponding to $\Delta Y_{PSF} \sim 3.2$. We used the stellar models from Castelli & Kurucz (2004) to fit the literature photometry of HIP 82885, including extinction given its distance of ~ 850 pc (van Leeuwen 2007). This yielded an apparent Y mag of ~ 8.2 , which corresponds to the companion having $Y \sim 11.4 \pm 0.5$. This is marginally (1.7σ) fainter than the apparent magnitude of the companion at H band (10.5 ± 0.2 ; Biller et al. 2012).

We also note that Fig. 4 shows that the companion is clearly extended in the radial direction, compared to the scaled artificial PSF inserted 180° away. While not convincing on its own, this lends credence to the notion that an additional signal resides *outside* the location of

HD 142527B.

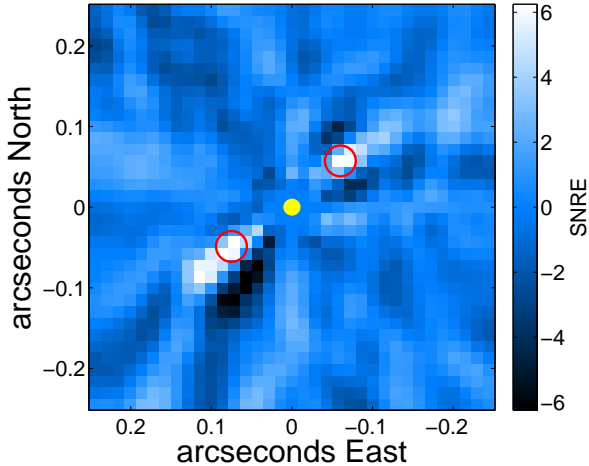


FIG. 4.— SNRE map of the total intensity image including the inserted and recovered scaled PSF. The red circles mark the locations of the real and artificial sources. Residual signal is located outside the position of HD 142527B, whereas no similar signal is seen near the artificial source on the opposite side of the star.

3.3. Polarization fraction near the companion

We next computed the polarization fraction near the companion, since this can be informative of dust grain properties (Perrin et al. 2009; Graham et al. 2007; and references therein). Typically one computes the ratio $p = P/I$, where P is the image of the source in polarized light and I is the image of the source in total intensity. Normally, for a disk of dust around a single central star, one performs PSF subtraction in total intensity to remove the star light and thus compute I (e.g., Perrin et al. 2009; Avenhaus et al. 2014). In our case, the polarized source is around the *secondary*. This makes computing p problematic because it is difficult to subtract the total intensity of the companion itself without also subtracting the circumsecondary source. Nonetheless, we can still compute a lower limit, p_{min} , recognizing that the companion’s photospheric light is included. We accomplished this as follows: we considered P to be our final polarized intensity image of the offset source (Fig. 2b), and I to be our final total intensity image of the companion (Fig. 1c). As Fig. 4 shows, this image also contains scattered light extending away from the companion at the location of the polarized source. We computed P/I and measured p_{min} as the median in a 3×3 pixel box centered on the peak location of the polarized source. By inserting and recovering artificial sources, we verified that the attenuation due to ADI+PCA was comparable in both the P and I images, meaning no additional flux-correction factors were required. Therefore $p_{min} \approx 10\%$.

4. DISCUSSION AND SUMMARY

We have detected HD 142527B in total intensity at Y band at approximately its expected location. Its brightness is marginally fainter than at H band, perhaps suggesting that the companion is red at $Y - H$ like it is at $1.6\text{--}4 \mu\text{m}$ (Biller et al. 2012). We also detected a point-source in polarized light whose projected separation from

the primary is larger than the companion’s by ~ 2.7 AU (at $>2\sigma$ confidence). The detection of polarized light is a strong indicator of scattering dust particles. This dust is mostly scattering light from the primary, since the Y band flux received from the primary at the polarized source location is ~ 3 times higher than the flux received from the companion. Assuming the polarized source is spatially separated from the companion, this system may resemble a scaled up version of the LkCa 15 system, which is thought to host a young protoplanet separated from one or more dust clumps (Kraus & Ireland 2012).

The detection of polarized light near HD 142527B complicates its classification. Because the scattering dust is likely falling onto or orbiting the companion, it is possible that this dust contributes to the total intensity that has been directly detected at other wavelengths. If this is the case, the reported masses for the companion ($0.1\text{--}0.4 M_{\odot}$; Biller et al. 2012; Close et al. 2014) should be viewed as *upper* limits only. To determine the lower limit on the companion mass, one would need to detect and subtract the contribution to the total light from the dust near the companion. Unfortunately, this is a daunting task because PSF subtraction on a faint *secondary* at $< 0''.1$ is extremely difficult.

Nonetheless, we can still make some inferences on the physical processes that would be occurring in the circumsecondary environment depending on the mass of the companion. Indeed the disk morphology and gap width depend uniquely on the binary mass ratio and orbital eccentricity (Pichardo et al. 2008). If the companion is a low-mass star, then most of the light we see at Y band is coming from the companion’s photosphere, rather than the circumsecondary material. This in turn means that the true fractional polarization, p , would be much larger than $p_{min} \approx 10\%$. Since the outer disk also has large fractional polarizations ($\sim 20\text{--}50\%$ (Avenhaus et al. 2014)), this could indicate that the dust near the companion is similar to the dust in the outer disk. Depending on the orbital eccentricity of the companion, which can be constrained in a few more years, the dust near the companion might have been swept up from the outer disk along its orbit.

If, on the other hand, the companion is a gas giant planet or protoplanet, then the light we see at Y band (and at other wavelengths) is dominated by the circumsecondary dust, meaning the true fractional polarization would be small. This could indicate that the dust near the companion is *different* from the dust in the outer disk. The dust near the companion might then originate from the inner disk. This would suggest that dust grains from the outer disk are not following the gap-crossing gas (Casassus et al. 2013b). It might also mean that multiple planets are responsible for the observed wide disk gap, since photoevaporation is unlikely in this accreting system (Dodson-Robinson & Salyk 2011).

This intriguing system and its multiple components must be monitored and observed at additional wavelengths (e.g., with GPI, MagAO, and/or SPHERE) so that these differing physical processes can be distinguished. The detection of the companion and nearby dust in polarized light in just 12 minutes of integration at $< 0''.1$ suggests that ODD in concert with ADI+PCA can be a powerful tool for detecting dust around off-axis

point-sources. In particular, older planets with their own circumplanetary disks or rings may even be detectable by current facilities like GPI in the coming years.

We are grateful to Marshall Perrin, Fredrik Rantakyro,

Pascale Hibon, and the GPI science and instrument teams for their help obtaining, processing, and reducing the data. We thank the referee for helpful comments and suggestions.

REFERENCES

- Avenhaus, H., Quanz, S. P., Schmid, H. M., et al. 2014, *ApJ*, 781, 87
- Biller, B., Lacour, S., Juhász, A., et al. 2012, *ApJ*, 753, L38
- Canovas, H., Ménard, F., Hales, A., et al. 2013, *A&A*, 556, A123
- Casassus, S., Hales, A., de Gregorio, I., et al. 2013a, *A&A*, 553, A64
- Casassus, S., van der Plas, G., M, S. P., et al. 2013b, *Nature*, 493, 191
- Castelli, F., & Kurucz, R. L. 2004, *ArXiv Astrophysics e-prints*, astro-ph/0405087
- Close, L. M., Males, J. R., Morzinski, K., et al. 2013, *ApJ*, 774, 94
- Close, L. M., Follette, K. B., Males, J. R., et al. 2014, *ApJ*, 781, L30
- Dodson-Robinson, S. E., & Salyk, C. 2011, *ApJ*, 738, 131
- Fukagawa, M., Tamura, M., Itoh, Y., et al. 2006, *ApJ*, 636, L153
- Graham, J. R., Kalas, P. G., & Matthews, B. C. 2007, *ApJ*, 654, 595
- Hinkley, S., Oppenheimer, B. R., Soummer, R., et al. 2009, *ApJ*, 701, 804
- Honda, M., Inoue, A. K., Fukagawa, M., et al. 2009, *ApJ*, 690, L110
- Houk, N. 1978, Michigan catalogue of two-dimensional spectral types for the HD stars
- Kokubo, E., & Ida, S. 2002, *ApJ*, 581, 666
- Konopacky, Q. M., Thomas, S. J., Macintosh, B. A., et al. 2014, *ArXiv e-prints*, arXiv:1407.2305
- Kraus, A. L., & Ireland, M. J. 2012, *ApJ*, 745, 5
- Kuhn, J. R., Potter, D., & Parise, B. 2001, *ApJ*, 553, L189
- Macintosh, B. A., Anthony, A., Atwood, J., et al. 2012, in *Society of Photo-Optical Instrumentation Engineers (SPIE) Conference Series*, Vol. 8446, Society of Photo-Optical Instrumentation Engineers (SPIE) Conference Series
- Marois, C., Lafrenière, D., Doyon, R., Macintosh, B., & Nadeau, D. 2006, *ApJ*, 641, 556
- Mendigutía, I., Fairlamb, J., Montesinos, B., et al. 2014, *ArXiv e-prints*, arXiv:1405.7378
- Nagel, E. 2014, *RMxAA*, 50, 41
- Perrin, M. D., Schneider, G., Duchene, G., et al. 2009, *ApJ*, 707, L132
- Pichardo, B., Sparke, L. S., & Aguilar, L. A. 2008, *MNRAS*, 391, 815
- Soummer, R., Pueyo, L., & Larkin, J. 2012, *ApJ*, 755, L28
- van Leeuwen, F. 2007, *A&A*, 474, 653
- Verhoeff, A. P., Min, M., Pantin, E., et al. 2011, *A&A*, 528, A91